Marine Geophysical Researches **23:** 109–123, 2002.

Gas hydrate and free gas distribution from inversion of seismic data on the South Shetland margin (Antarctica)

Umberta Tinivella*, Flavio Accaino and Angelo Camerlenghi
*Istituto Nazionale di Oceanografia e di Geofisica Sperimentale, Trieste, Italy; *Author for correspondence (Fax: +39 40 327307; E-mail: utinivella@ogs.trieste.it)*

Received 30 November 2001; accepted 27 August 2002

Abstract

Travel-time inversion is applied to seismic data to produce acoustic velocity images of the upper 800 m of the South Shetland margin (Antarctic Peninsula) in three different geological domains: (i) the continental shelf; (ii) the accretionary prism; (iii) the trench. The velocity in the continental shelf sediments is remarkably higher, up to 1000 m/s at 600–700 m below seafloor, than that of the other two geological domains, due to the sediment overcompaction and erosion induced by the wax and waning of a grounded ice sheet. Pre-stack depth migration was applied to the data in order to improve the seismic image and to test the quality of the velocity fields. Where the Bottom Simulating Reflector (BSR) is present, positive and negative velocity anomalies were found with respect to a reference empirical velocity profile. The 2D-velocity section was translated in gas hydrate and free gas distribution by using a theoretical approach. The analysis revealed that the BSR is mainly related to the presence of free gas below it. The free gas is distributed in the area with variable concentration and thickness, while the gas hydrate is quite uniformly distributed across the margin.

Introduction

The regional distribution of Bottom Simulating Reflectors (BSRs) generated by gas hydrates and free gas trapped below the hydrate stability zone provides an important clue to their origin, which is always in some way related to the geological setting of the area of occurrence. In order to improve the interpretation of the genesis of these hydrocarbon gas accumulations, a question must be asked on which degree of accuracy the spatial distribution of gas in either phase and its volumetric abundance have to be known. Drilling through a hydrate zone often yields a qualitative assessment of hydrate content because of the difficulties in preserving the sample at in situ conditions. In addition, difficulty arises in extrapolating information laterally from well site location because of the following facts:

(1) the occurrence of a BSR on seismic profiles is certainly an indication of occurrence of hydrates. However, the seismic appearance of BSR is highly dependent on acquisition methods (Wood and Ruppel, 2000);

(2) the absence of a BSR on a seismic profile does not imply absence of gas hydrates in the sediments (Paull et al., 2000);

(3) other surface indications of gas venting, provided by side scan sonar images and visual seafloor observations, cannot, in general, discriminate by themselves between gas occurrence in the form of hydrates or free gas (Miles, 2000).

By inverting elastic equations of the compressional wave velocity obtained downhole via a Vertical Seismic Profile, or a Sonic Log, attempts have been made recently (Helgerud et al., 1999; Tinivella, 1999; Tinivella and Lodolo, 2000) to estimates gas hydrates and free gas concentrations downhole that match satisfactorily the plot of concentrations obtained through chlorinity dilution in core samples. The technique of full waveform inversion applied by Yuan at al. (1999) on the Cascadia margin, and by Andreassen et al. (2000) to the Storegga Slide Area allows a reconstruction of the velocity profile in one dimension. Correlation with VSP data supports this evidence. Additionally, the resistivity log in conjunction with laboratory data can be used for the punctual estimation of hydrates, as demonstrated recently by Hyndman et al. (1999) on the Vancouver margin.

A step forward is now the propagation in two dimensions, along a seismic profile, of the quantitative one-dimensional information obtained on borehole location (Tinivella and Carcione, 2000). Fields of dis-

tribution of the parameters considered (velocity, or resistivity as well as several other physical properties) must be reconstructed as accurately as possible. If velocity is considered, the seismic data must be multichannel seismic profiles with adequate velocity information contained in appropriate offset range. The velocity field can be later inverted as hydrate and free gas concentration by extrapolation of the physical properties derived locally.

In this paper, we analyse the BSR identified on the South Shetland continental margin (Antarctic Peninsula; Tinivella et al., 1998). We determine a detailed velocity field by using an inversion code (Zelt and Smith, 1992 and Geodepth©, Paradigm Geophysical) in three different geological domains:
(1) the continental shelf where no BSR is present;
(2) the accretionary wedge where a strong BSR is present;
(3) in the trench, where no BSR is present.

Pre-stack depth migration is applied to improve the seismic sections and to verify the velocity models. Anomalies in the 2D velocity fields where the BSR is present are translated in two-dimensional fields of distribution of gas hydrate and free gas concentrations of volume.

Regional geological setting

The South Shetland margin is a convergent plate boundary where the Phoenix oceanic plate is subducted beneath the continental block of the Antarctic plate, in which a typical trench-accretionary prism-fore arc basin sequence can be recognised (Maldonado et al., 1994; Kim et al., 1995). Extension at the Phoenix ridge ceased about 2.3–3.3 Ma. Therefore, subduction is now believed to take place as a consequence of the sinking and rollback of the oceanic lithosphere (Larter and Barker, 1991; Kim et al., 1995). A magmatic arc, the South Shetland Islands has formed during the phases of active subduction, while presently volcanic activity is concentrated in the areas of crustal extension of the Bransfield back arc basin. The margin is confined laterally by two major oceanic fracture zones, Hero (SW) and Shackleton (NE), which intersect the continental lithosphere as they meet the continental margin. For a deeper analysis of the local geological context, see the bibliographic references cited above.

For the purpose of this paper, it is important that the reader recognises the complexity of the geological environment, which is tectonically active and includes a variety of lithologies and styles of deformation. This setting contrasts, being more challenging in terms of data analysis and interpretation, with that of passive continental margins in which gas hydrates are also commonly found, characterised by lateral uniformity of lithologic formation and, generally, little deformation.

Seismic data

A strong BSR was identified on multichannel seismic reflection profiles acquired during the Austral summers 1989/1990 (lines IT90A43 and IT90A44, dashed lines in Figure 1) and 1996/1997 (solid lines in Figure 1) on the South Shetland Margin (Lodolo et al., 1993; Lodolo et al., 2002). In the first acquisition leg, the energy source was two air-gun arrays of 15 guns each with a total volume of 45 litre. The shot spacing was 50 m, the streamer was 3000 m long with a hydrophone group interval of 25 m, and the sampling interval was 4 ms. The second leg was characterised by an energy source of two GI guns with a total volume of 4 litres firing every 25 m. The streamer was the same of the previous survey. The sampling interval was 2 ms. We also deployed an Ocean Bottom Seismometer (OBS; solid circle in Figure 1) where the BSR signature is particularly evident (Tinivella and Accaino, 2000).

After the reconstruction of the velocity field from seismic inversion (see below), we applied the pre-stack depth migration to the data corrected only by the spherical divergence and absorption compensation.

Acoustic velocity fields and inversion methods

We analysed parts of seismic profiles (see thick solid lines in Figure 1) with the aim of obtaining the compressional velocity field in the area. In particular, we selected a part of (i) the continental shelf (line IT90A43), (ii) the accretionary wedge (line I97213), and (iii) the trench (line IT90A43).

We used two codes to obtain the velocity field: the Zelt and Smith (1992) method and the commercial Geodepth© package.

The procedure of the first code basically consists of two steps: identification of acoustic discontinuities (horizons) in the pre-stack domain and determination of relative travel times for various source-receiver

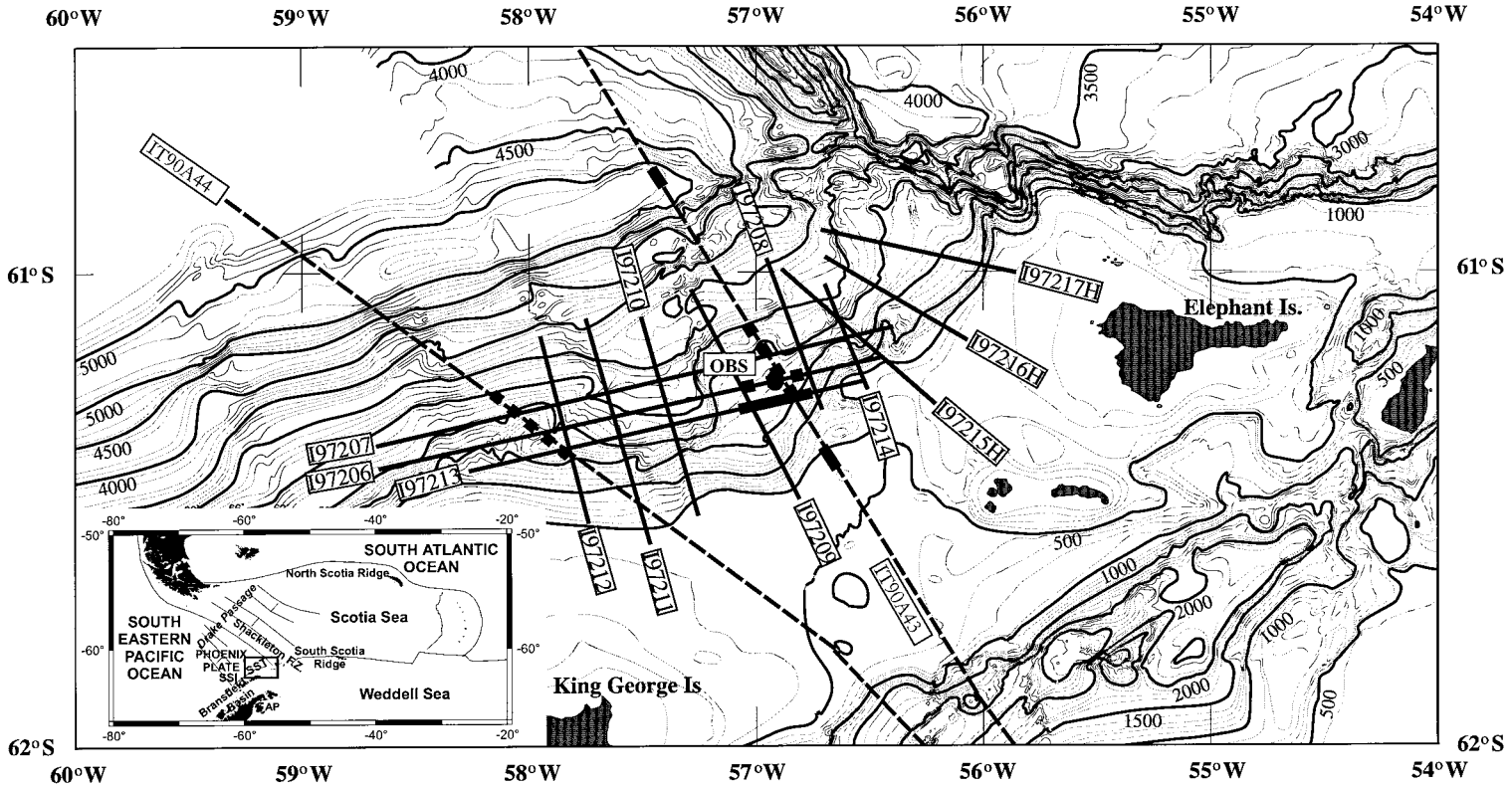

Figure 1. Bathymetric map of the South Shetland Margin (Klepeis and Lawver, 1996), with location of the two profiles acquired in 1989/90 (dashed lines) and the seismic grid acquired in 1996/97. The thick dotted and the solid segments indicate the previous and here-presented analyses respectively. The circle shows the OBS location. Insert: General tectonic map of the Scotia Sea region. SSI = South Shetland Islands; SST = South Shetland Trench; AP = Antarctic Peninsula. Box indicates the study area.

positions (picking of horizon); local velocity model estimation by inversion. In essence, the inversion of the travel time employs a forward ray-tracing step and damped least-squares inversion step to modify the model parameters (velocities and/or depth of layers) by minimising the difference between the observed and predicted travel times.

The second procedure used is the inversion with the Geodepth© software. Firstly, we interpreted the stack section by picking the main reflectors. On the basis of the picks, the algorithm identifies the events in the pre-stack domain using coherence analysis. The inversion algorithm uses ray tracing to compute the move-out curves and we choose the maximum semblance between the data and predictions. This process is performed within a time window around the common mid points predicted by the ray-tracing algorithm. Next, a depth section is generated using the interval velocities obtained with the inversion technique. The model can be updated by using the residual moveout corrections applied to image gathers (the output of the pre-stack depth migration) as local method and reflection tomography as a global method as described below.

The residual moveout is the first step used to update the initially picked velocity function. The degree of non-flatness of an event on image gathers yields a qualitative estimation of the error in the determination of the model. In fact, the flatness is an indication of the accuracy of the velocity field associated with the layer above the layer boundary that is represented by that event (see for example Yilmaz, 2001). The steps to make the residual moveout correction by using Geodepth© software are as follows: (a) perform a pre-stack depth migration by using the velocity model to obtain the image gathers; (b) convert the image gathers from depth to time; (c) assume that the residual moveout of events in time is parabolic and compute a semblance spectrum; (d) apply residual moveout correction; (e) compute new velocity model. The residual moveout analysis of image gathers and the update of velocity-depth model should be performed iteratively until the velocity-depth model and the depth image are consistent.

Finally, the model is refined by using the horizon-based global-depth tomographic algorithm, using depth delays. The reflection traveltime tomography is based on perturbing the initial model parameters by a small amount and then matching the change in traveltimes to the traveltime measurements made from residual moveout analysis of image gathers. The tomographic scheme can be summarised as follow: (a) generate the image gathers; (b) convert the image gathers from depth to time; (c) compute the horizon-consistent residual moveout; (d) pick the residual moveout profiles; (e) update the model by using the tomographic algorithm (see for example Yilmaz, 2001). The tomographic update is the last step we use to determine the final velocity model.

The main advantage to use Geodepth© is that we pick the stack section instead of the pre-stack data. In this way, picking is easier for horizons not evident in the pre-stack data (i.e. the base of the free gas layer, the so-called BGL). On the other hand, the resolution of the velocity model by using the first code is better, and there is a quantitative control of the quality of the final velocity model, instead of a qualitative control provided by the flatness of horizons in the image gathers.

Velocity model

Figure 2 shows the velocity model obtained in the continental shelf, where the BSR is not present. The result indicates that the velocity ranges from 1750 to 3000 m/s from the sea bottom to 750 m depth, increasing with depth following the geometry of topset reflectors subparallel to the seafloor reflector. The overall high velocity found even at shallow sub-bottom depth is produced by overcompaction of glacial sediments and glacial erosion by the grounded ice sheet that modelled the margin architecture after the onset of glacial conditions at the Antarctic Peninsula Pacific margin, presumably since the late Miocene (Barker et al., 1999). This velocity field is in agreement with other analyses performed on topset continental shelf sequences of other parts of the Antarctic margin (Cochrane and Cooper, 1991; Shipboard Scientific Party, 1999; Tinivella et al., 2001).

Within the accretionary prism, the selected part of the line I97213 (Figure 3) presents two different acoustic characteristics of the BSR at either side of a velocity high located approximately in the middle of the section. West of this structure, the BSR is only weakly evident, discontinuous and offset by faults; conversely, to the East, the BSR is strong and continuous. We picked the sea floor, the BSR, three and four reflectors between the two in the East and West parts respectively, the base of free gas reflectors (BGR according to Tinivella et al., 1998), and a basement reflector. The velocity model above the BSR was ob-

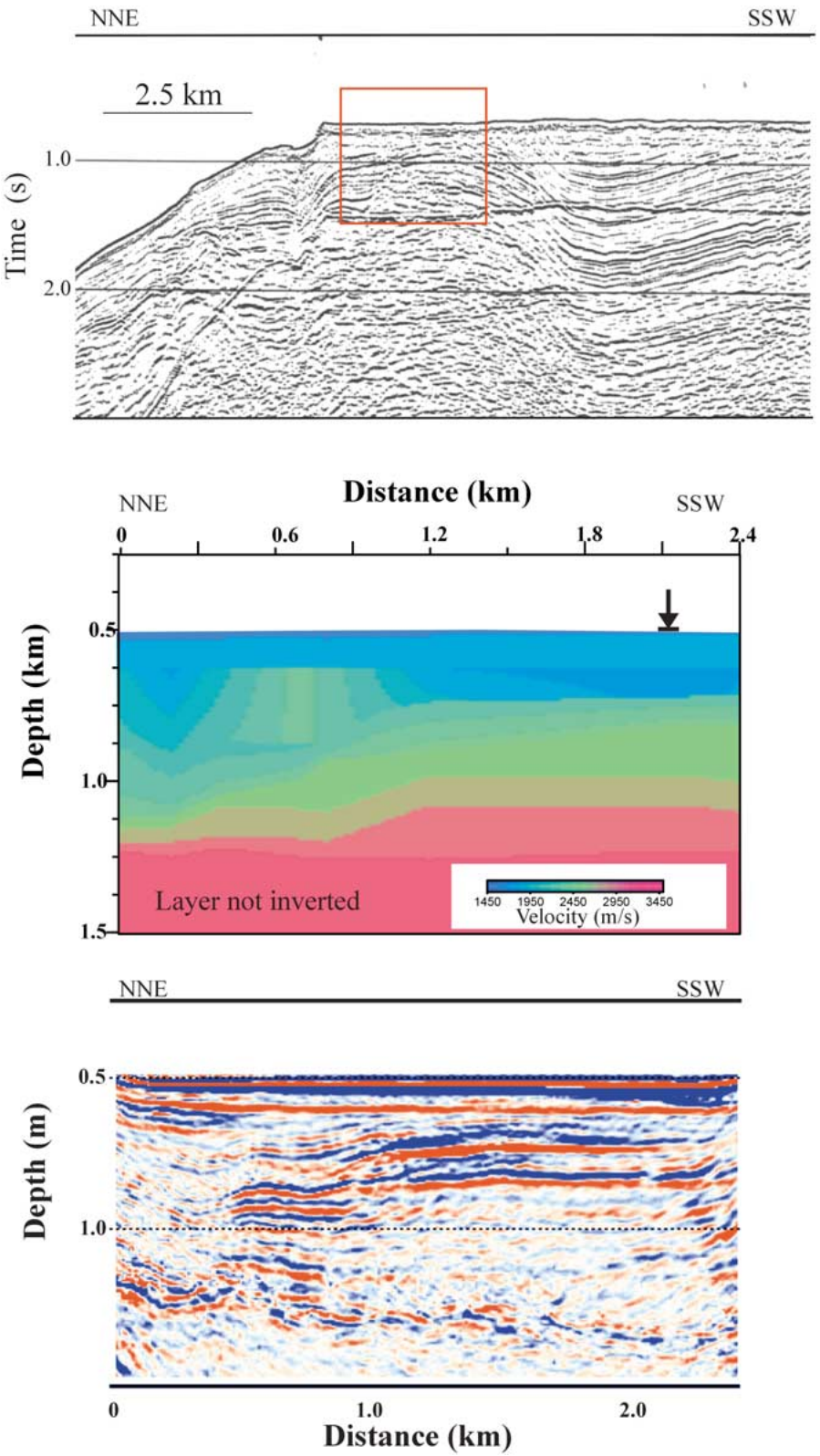

Figure 2. Top: stack image of the continental shelf (line IT90A43); the box indicates the analysed seismic part. Middle: velocity model obtained after inversion. The arrow indicates the selected location of velocity profile (see Figure 8). Bottom: pre-stack depth migrated seismic section.

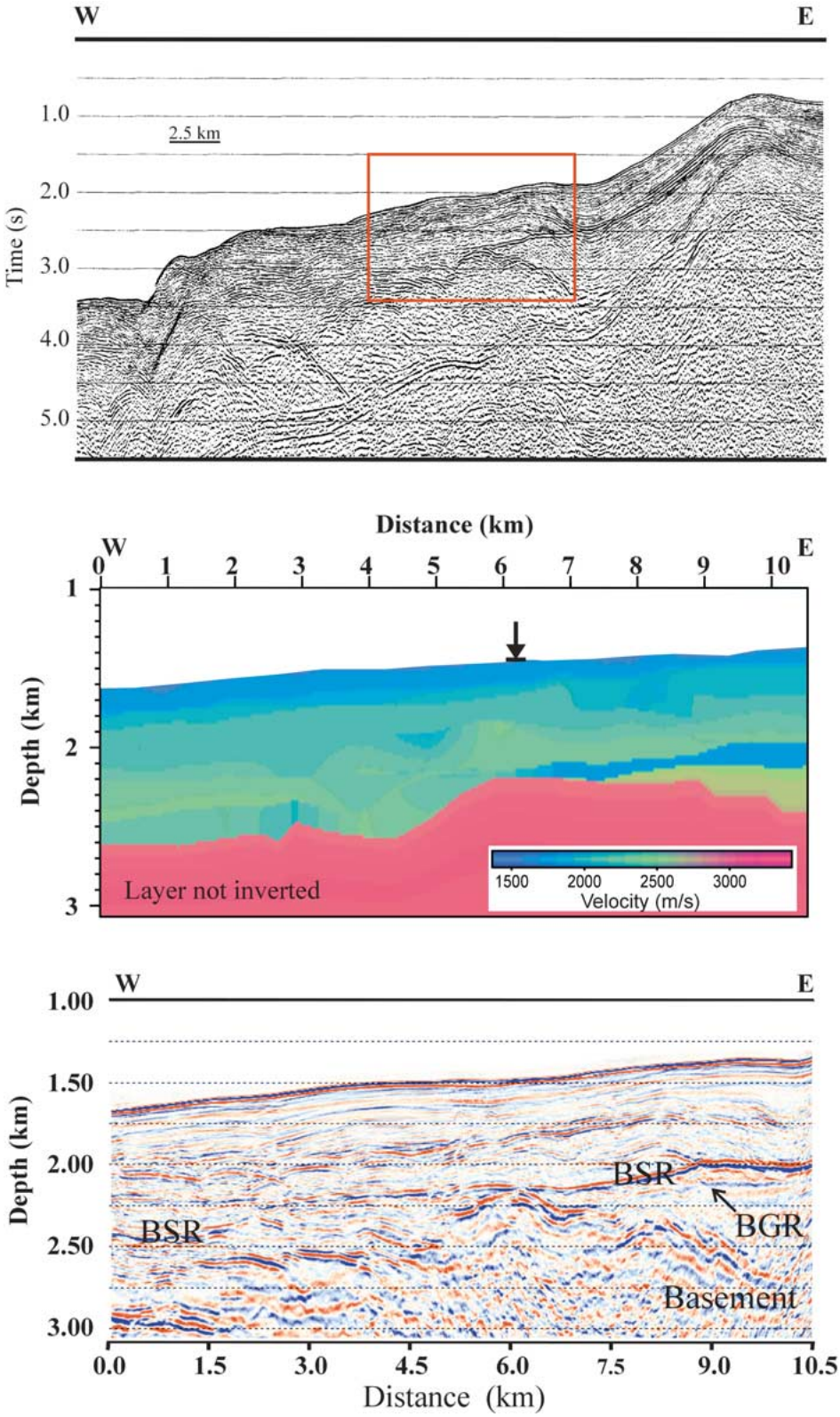

Figure 3. Top: stack profile of the selected part of line I97213; the box indicates the analysed seismic part. Middle: velocity model obtained after inversion. The arrow indicates the selected location of velocity profile (see Figure 8). Bottom: pre-stack depth migrated seismic section.

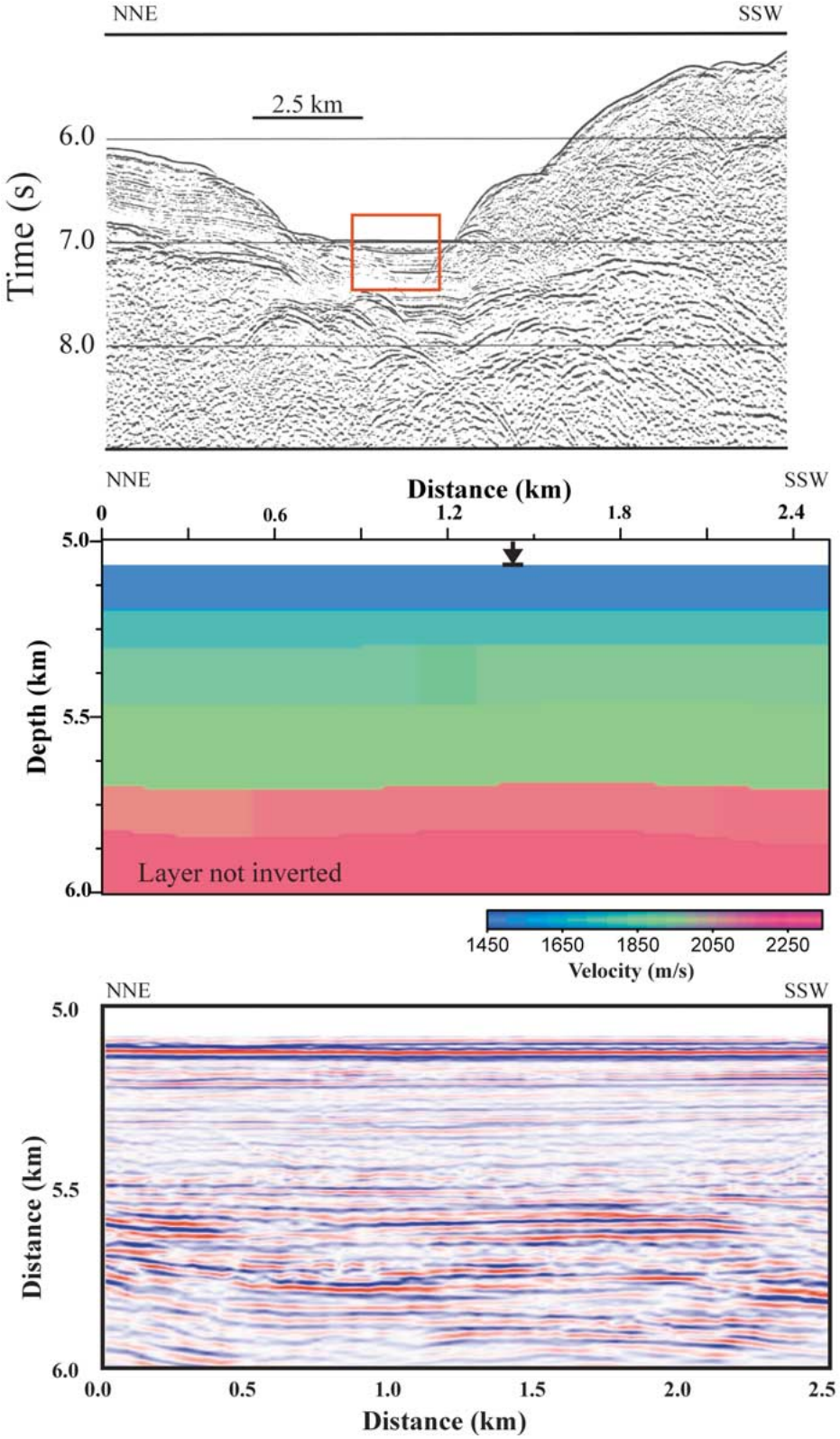

Figure 4. Top: stack image of the trench (line IT90A43); the box indicates the analysed seismic part. Middle: velocity model obtained after inversion. The arrow indicates the selected location of velocity profile (see Figure 8). Bottom: pre-stack depth migrated seismic section.

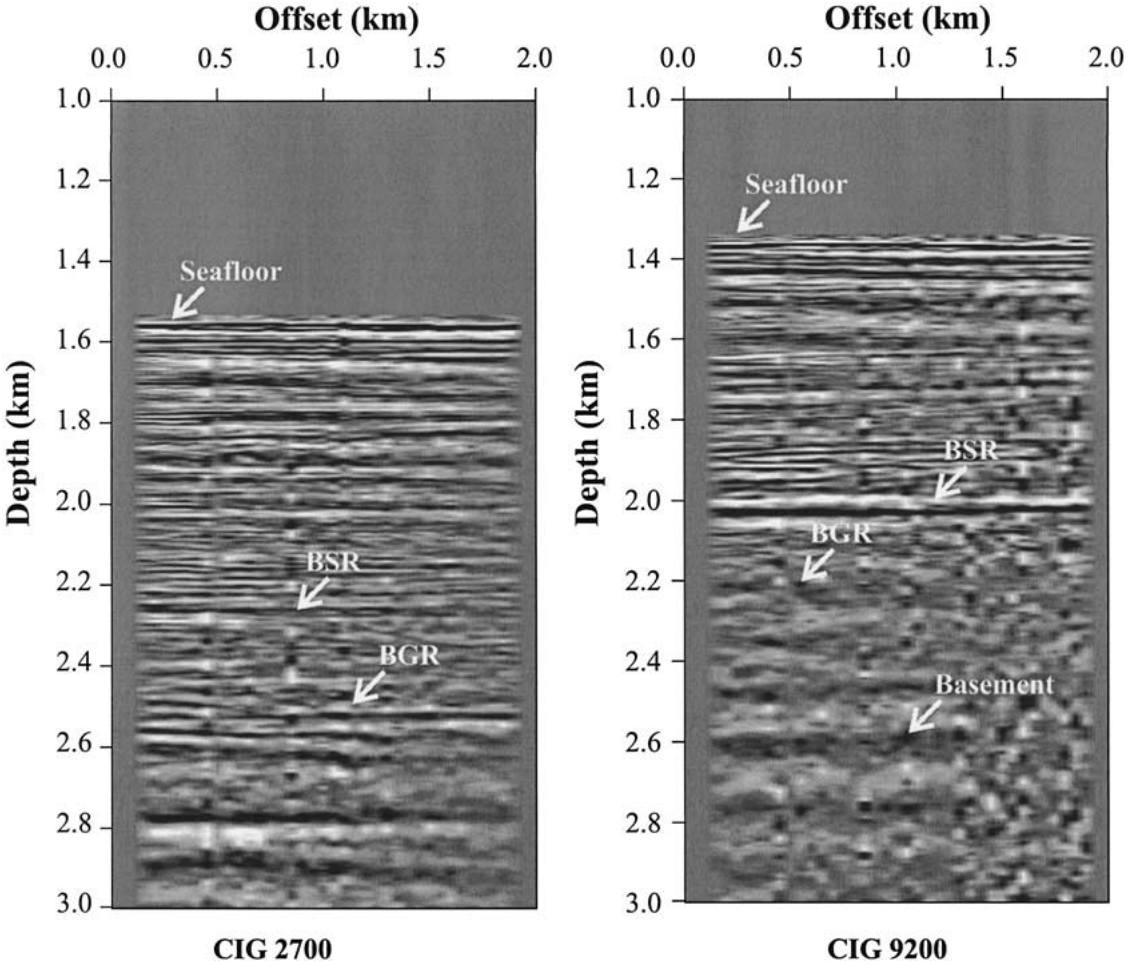

Figure 5. Common image gather obtained at 2700 m (left) and 9200 m (right), line I97213.

tained with the Zelt and Smith approach (1992). The Geodepth© software is used to obtain the initial model of the two last horizons and successively the velocity and the geometry were refined with the first code.

The final result, shown in Figure 3, indicates that the velocity increases from 1600 at the sea bottom to 2250 m/s at the BSR, which lays approximately 600 m below seafloor. The interval overlaying the BSR is characterised by remarkable lateral variations in interval velocity between 2000 and 2250 m/s. Where the BSR is strong and continuous (to the East of the velocity high) a low-velocity zone of average interval velocity of 1600 m/s between the BSR and the BGR, indicates the presence of free gas-bearing sediments, with an average thickness of about 100 m. Where the BSR is discontinuous, the velocity inversion below the BSR is less pronounced, from 2300 to 1900 m/s. In the deepest layer, not inverted, we introduced a vertical velocity gradient to improve the results of the pre-stack depth migration.

In the subduction trench, where the BSR is not present, the inversion of the data (Figure 4) indicates a normally compacted sedimentary sequence in which the vertical velocity gradient follows subparallel filling of a basin. We observe no lateral velocity variations. The velocity is lower than that observed on the shelf and in the accretionary complex.

Pre-stack depth migration

In order to enhance the seismic images and to test the velocity model obtained by inversion, we performed a pre-stack depth migration with the Kirchhoff method. Figures 2–4 show the resulting seismic sections. As earlier underlined, the pre-stack depth migration can

Table 1. List of parameters in equation (1) and variation of material properties vs. depth (after Tinivella, 1999).

ϕ	Porosity
ϕ_s	Solid proportion
ϕ_h	Gas hydrate proportion
ϕ_w	Water proportion
ϕ_g	Free gas proportion
$\phi_s + \phi_w + \phi_g = 1$	
$\phi_s + \phi_h + \phi_w = 1$	
$c_h = \phi_h/(\phi_h + \phi_w)$	Gas hydrate concentration
$s_s = \phi_s/(\phi_s + \phi_h)$	Grain saturation
$s_h = \phi_h/(\phi_h + \phi_s)$	Gas hydrate saturation
$s_w = \phi_w/(\phi_w + \phi_g)$	Water saturation
$s_g = \phi_g/(\phi_w + \phi_g)$	Free gas saturation
$\phi_{eff} = (1 - c_h)\phi$	Effective porosity
C_s	Grain compressibility
C_h	Gas hydrate compressibility
C_w	Water compressibility
C_g	Free gas compressibility
C_b	Compressibility of the solid phase
C_f	Compressibility of the fluid phase
$C_p = (1 - \phi/\phi_0)/\mathrm{P_d}$	Pore compressibility
ϕ_0	Porosity at the sea bottom
$\mathrm{P_d}$	Differential pressure
$C_m = (1 - \phi_{eff})C_b + \phi_{eff}C_p$	Compressibility of the matrix
$\beta = C_b/C_m$	
ρ_s	Grain density
ρ_h	Gas hydrate density
ρ_w	Water density
ρ_g	Gas density
$\rho_b = s_s\rho_s + s_h\rho_h$	Density of the solid phase
$\rho_f = s_w\rho_w + s_g\rho_g$	Density of the fluid phase
$\rho_m = (1 - \phi_{eff})\rho_b + \phi_{eff}\rho_f$	Average density
μ_{sm0}	Solid matrix shear modulus (no cementation)
μ_{smKT}	Kuster and Toksöz's shear modulus (Kuster and Toksöz, 1974)
$\mu_{sm} = (\mu_{\mathrm{smKT}} - \mu_{\mathrm{sm0}})[\phi_{\mathrm{h}}/(1-\phi_s)]^{3.8} + \mu_{\mathrm{sm0}}$	Solid matrix shear modulus (percolation theory)
$\mu_s = \mu_{\mathrm{sm0}}/(1 - \phi)$	Grain rigidity
μ_h	Gas hydrate rigidity
$\mu = (\phi_s + \phi_h)(\phi_s s_s/\mu_{sm} + s_h/\mu_h)^{-1}$	Average rigidity of the skeleton
K	Coupling factor

be used to determine the reliability of the velocity model obtained from the traveltime inversion. In fact, if the velocity-depth model and the pre-stack depth migration section are consistent, this implies that we have a very accurate velocity field (Kim et al., 1996). So, the satisfactory results obtained for all the studied sections, confirm that the velocity structures is reliable.

Another important test that we performed to check velocity accuracy, is the analysis of the common image gathers. Figure 5 shows the common image gathers at two locations (line I97213), in particular in the West

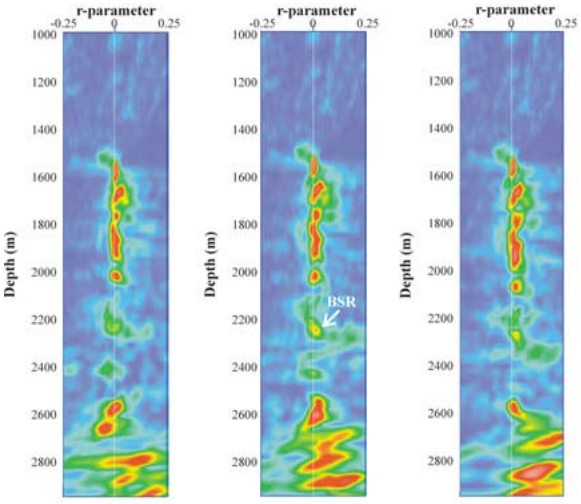

Figure 6. Semblance of the residual velocity analysis for the common image gather located at 2700 m (line I97213), obtained considering the inverted velocity perturbed below the sea floor of -5% (panel in the left), the inverted velocity (panel in the middle) and the inverted velocity perturbed below the sea floor of $+5\%$ (panel in the right).

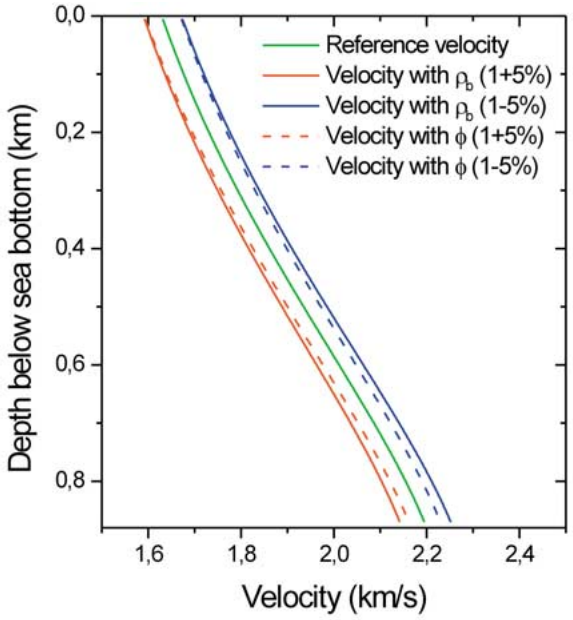

Figure 7. Influence on the velocity caused by the increase/decrease of the porosity ϕ and the average density ρ_b of 5%. The green line is the reference velocity. The red/blue solid lines indicate the velocity evaluated increasing/decreasing the average density of 5%. The red/blue dashed lines indicate the velocity evaluated increasing/decreasing the porosity of 5%.

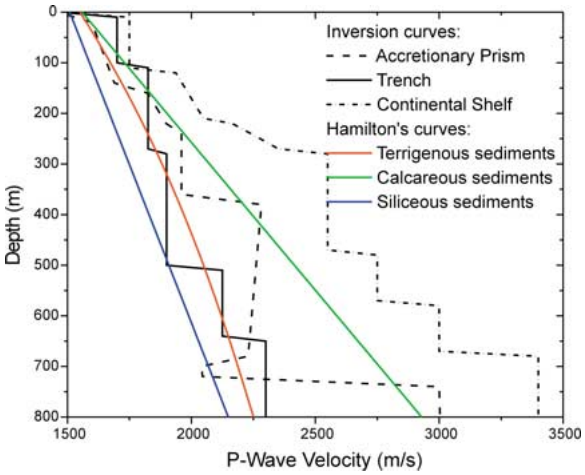

Figure 8. Comparison between Hamilton's velocity (red line: terrigenous sediments; blue line: siliceous sediments; green line: calcareous sediments; Hamilton, 1978) and the compressional velocity profiles obtained from the inversions at selected location in the continental shelf (dashed-dotted line), the accretionary prism (dashedline), and in the trench (black solid line).

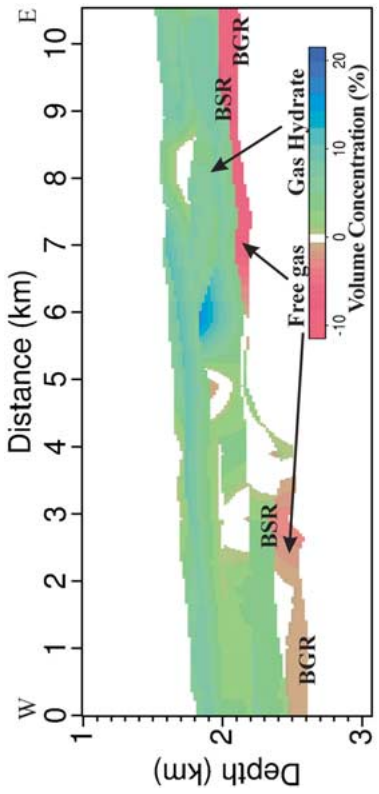

Figure 9. Distribution of the gas hydrate and free gas in the accretionary prism. Positive values are the gas hydrate concentration, while the negative concentrations are related to the percentage of volume occupied by free gas.

part (2700 m in the model) and in the East part of the section, where the BSR is strong (9200 m in the model). The flatness of the reflections indicates the reliability of the velocity model.

The semblance of the residual velocity analysis is useful to check the velocity error. In fact, if the energy is focalised across the zero, this signifies that the velocity is corrected (i.e., Yilmaz, 2001). For this reason, we evaluated the semblances of the residual velocity analysis, considering three different velocity fields: the inverted velocity field and the inverted velocity field perturbed of $\pm 5\%$, fixing the seawater velocity. An example of semblance (at 2700 m in the velocity model) is shown in Figure 6. Figure 6 left and 6 right are obtained perturbing the final velocity model below the sea floor of -5% and $+5\%$ respectively, while Figure 6 middle shows the semblance considering the velocity field obtained from the inversion procedure. The BSR is located at about 2300 m, and the basement is about 2500 m depth. We can observe that the semblance across the BSR, where we focused our analysis, is the best in the middle panel, which is obtained with the inverted velocity. In fact, the energy at the BSR is more focalised, and the energy between the BSR and the basement is more evident than in the other two panels. These results allow us to affirm that our velocity fields have accuracy of the order of magnitude of 5%.

We focused our attention to line I97213 (Figure 3), where the pre-stack depth migration outlines the presence of geological structures such as reverse faults in the deeper units of the accreted terrains, and gentle folds particularly evident in the sedimentary units overlying the faulted terrains. Note that the BSR appears to cut across folded structures to the East of the section, while it is clearly interrupted in correspondence of reverse folds that cause a slight vertical offset (at about 3.5 km in the model). The migrated seismic section outlines the BGR in the eastern part, where it is not so evident in the pre-stack data (see top of Figure 3).

Theoretical model for gas hydrate- and free gas-bearing sediments

In order to quantify the concentrations of gas hydrate and free gas in the pore space, we used Biot-Geertsma-Smit equations (see for example Domenico, 1977) to model the acoustic properties of different layers associated with the BSR (Tinivella, 1999). This approach models the different layers associated with the BSR (two solids -grains and clathrates- and two fluids –water and free gas-) including an explicit dependence on differential pressure and depth, and the effects of cementation by hydrate on shear modulus of the sediment matrix by using the percolation model. The theory gives both compressional and shear wave velocities. The physical parameters necessary to evaluate the velocities (porosity, compressibility, rigidity, density, frequency dependence) can be determined from available lithostratigraphic information, and experimental data sets (Hamilton's curves).

The compressional wave velocity is expressed as (see explanation of symbols and variations of material properties vs. depth in Table 1):

$$V_p = \left\{ \left[\left(\frac{1}{C_m} + \frac{4}{3}\mu \right) + \frac{\frac{\phi_{eff}}{k}\frac{\rho_m}{\rho_f} + \left(1 - \beta - 2 \cdot \frac{\phi_{eff}}{k}\right) \cdot (1-\beta)}{(1 - \phi_{eff} - \beta)C_b + \phi_{eff} C_f} \right] \cdot \frac{1}{\rho_m \left(1 - \frac{\phi_{eff}}{k}\frac{\rho_f}{\rho_m}\right)} \right\}^{1/2} . \quad (1)$$

The theoretical model here described was compared with the Biot-type three-phase theory (Tinivella and Carcione, 2000); the comparison shows that the two theoretical approaches are in very good agreement. The theory has been applied to verify the model and to estimate the gas hydrate and the free gas concentrations in three different areas: South Shetland margin (Tinivella and Accaino, 2000; Lodolo et al., 2002), Blake Ridge (Tinivella, 1999; Tinivella and Lodolo, 2000), and Cascadia margin (Tinivella and Carcione, 2000).

We can suppose four main relative distributions of free gas: (1) uniform, (2) 50% uniform and 50% random, (3) patchy and (4) random. In the first two cases, the velocity decreases fast with a small amount of free gas. In the two latter cases, the velocity decreases quite linearly versus free gas amount (Tinivella and Carcione, 2000). In this paper, we suppose the patchy distribution of free gas in the pore space, i.e. all water is concentrated in fully saturated patches and gas is concentrated in patches without water (see for details Hill, 1963 and Dvorkin et al., 1999).

Test of sensitivity

In order to determine the influence of each parameter regarding the estimate of gas hydrate and free gas content, we perturbed the main parameters (see Table 1)

Table 2. Variation of the average gas hydrate (ϕ_h) and free gas (ϕ_g) concentration versus the variation of the main parameters necessary to evaluate the theoretical velocity. The reference average concentration are $\phi_h = 6.0\%$ and $\phi_g = 4.3\%$.

Parameter	Variation of +5%	Variation of −5%
ϕ	$\phi_h = 7.1\%$ - $\phi_g = 4.3\%$	$\phi_h = 5.0\%$ - $\phi_g = 4.1\%$
ρ_b	$\phi_h = 7.2\%$ - $\phi_g = 4.0\%$	$\phi_h = 5.0\%$ - $\phi_g = 4.3\%$
μ_s	$\phi_h = 5.8\%$ - $\phi_g = 4.4\%$	$\phi_h = 6.1\%$ - $\phi_g = 4.1\%$
C_w	$\phi_h = 6.7\%$ - $\phi_g = 4.2\%$	$\phi_h = 5.3\%$ - $\phi_g = 4.2\%$
C_s	$\phi_h = 6.1\%$ - $\phi_g = 4.3\%$	$\phi_h = 5.8\%$ - $\phi_g = 4.3\%$
C_h	$\phi_h = 6.0\%$ - $\phi_g = 4.3\%$	$\phi_h = 5.9\%$ - $\phi_g = 4.3\%$
ρ_h	$\phi_h = 6.0\%$ - $\phi_g = 4.3\%$	$\phi_h = 5.9\%$ - $\phi_g = 4.3\%$

Table 3. Values of main parameters used in equation (1).

ϕ	$0.65\text{-}0.95z\text{+}0.34z^2$
C_s	0.027 $(\text{GPa})^{-1}$
C_h	0.119 $(\text{GPa})^{-1}$
C_w	Empirical formula (Riley and Chester, 1987)
C_g	42.4 $(\text{GPa})^{-1}$
$\rho_m(z)$	$(1530\text{+}1395z\text{-}0.617z^2)$ kg/m^3
ρ_h	920 kg/m^3
ρ_w	Empirical formula (Fofonoff and Millard, 1983)
ρ_g	88.48 kg/m^3
μ_{sm0}	See equation (2) in the text
μ_h	3.7 GPa
k	150

by ±5% and we observed the effect on the estimate of concentrations. Table 2 shows the change in the average estimate of gas hydrate and free gas – in the selected part of the line I97213 – with respect the change in the main parameters. The reference values are 6.0% for gas hydrate average concentration and 4.3% of volume for the free gas average amount (see next section). As expected, the results indicate that the most important parameters are the porosity and the average density. A variation of ±5% of the porosity and average density is translated in a variation of the gas hydrate concentration of about 1.2% by volume. Figure 7 shows the effect caused to increase/decrease the porosity and average density with a quantity equal to 5%; the velocity is changed of about few per cent. The major variation on free gas concentration we observed (−0.3% of volume) is caused by an increase of the average density.

The water and gas density, the gas and pore compressibility, and the hydrate shear modulus have no significant influence ($\ll$1% of volume concentration) on the estimate of gas hydrate and free gas amount.

If we have laboratory data, the uncertainties are expected to be less than 5% supposed in this test, and we can obtain the estimate with high precision. In the case presented in this paper, we have only seismic data and our error is related to the error in the estimate of reference velocity. Generally, the seismic velocity error is a few per cent, that corresponds roughly at parameter errors of few percent. So, from the results described in Table 2 and from the results obtained by the test velocity error (Figure 6), we can suppose that the errors in the gas hydrate and free gas estimate are in the order of magnitude of about 1.2% and 0.3% of volume respectively.

Estimate of gas hydrate and free gas concentration

To determine the reference velocity, i.e. the velocity versus depth in absence of hydrate and free gas, the velocity profiles obtained from the three inversions at selected location (see arrows in Figures 2–4) are compared in Figure 8 with the Hamilton (1978) velocities for terrigenous, calcareous, and siliceous sediments. Due to glacial compaction and erosion, the velocity obtained in the continental shelf is highest, while the other two profiles are in reasonable accordance with Hamilton's curve for terrigenous sediments, except in the layers just above and below the BSR. The parameters versus depth used (porosity, density, and compressibility) are taken from the Hamilton's data set for terrigenous sediments, except in the first 100 m of sediments, where the porosity and density were suitably modified to reproduce the trend of the trench velocity. Table 3 shows the values of the main parameters used to evaluate the velocity. The rigidity μ is evaluated according to the following formula:

$$\mu = (\rho\ \mathrm{Vp}^2(2\nu - 1)/(2\nu - 2))^{1/2}, \qquad (2)$$

where ρ is the density, Vp the reference compressional velocity, and ν the Poisson's ratio. We used the average Poisson's ratio (equal to 0.435) obtained by the travel time inversion of the shear energy observed in the horizontal components of the OBS (Tinivella and Accaino, 2000), using the Zelt and Smith (1992) method. The events observed in OBS data are associated with the converted reflected P wave at the BSR, with the converted reflected P wave at the BGR, and to the converted transmitted S wave at the BSR and then reflected at the BGR. Poisson's ratio obtained by the inversion of horizontal components of OBS data

is in very good agreement with the weighted average Poisson's ratio obtained by amplitude versus offset inversion of multichannel seismic data. The assumption of the value of Poisson's ratio is supported by the agreement between the two velocity fields (line I97206 and I97213) obtained above the BSR.

Firstly, we evaluate a reference velocity field in the area and compared it to the structure obtained from the travel-time inversion. Where discrepancies are found, we determine the concentration of hydrate or free gas increasing the concentrations in the theoretical formula [equation (1)]. Figure 9 shows the distribution of the two gas phases; positive values are the gas hydrate concentration, while the negative concentrations are related to the percentage of volume occupied by free gas. It is essential to consider the percentage of volume, when concentrations in different points are compared, as opposed to the percentage of pore space which does not give information about the real gas content, because of its dependence on porosity, i.e. depth. Highest concentration of gas hydrate (approximately 8–10% $\pm$ 1.2% of volume) and free gas (average concentration of 5.9% $\pm$ 0.3%) is found where the BSR is stronger, i.e. in the eastern part, while in the western part the average gas hydrate and free gas concentration is about 4.8% $\pm$ 1.2% and 3.1% $\pm$ 0.3% respectively. Note that the sediments just below the sea bottom are not hydrated. So, we found that also the free gas amount is dependent from acoustic characteristic of the BSR, and its thickness is variable.

Discussion and conclusions

Analyses of seismic data and the velocity structures allowed us to estimate the typical velocity curve of the sediments in the accretionary prism without gas hydrate and free gas and the consequent distribution of these gas phases, where anomalous velocities are found.

An average concentration of about 6.0% $\pm$ 1.2% and 4.3% $\pm$ 0.3% of hydrate and free gas of volume are obtained respectively. The hydrate is quite uniformly present in the investigated section, even though the positive velocity anomalies can be also related, in places, to geological structures. For instance, if the high velocity found in correspondence of the fold at about 6 km in Figure 3, is interpreted as being due to gas hydrates cementation, we obtain a concentration of about 15% $\pm$ 1.2%. This concentration is not acceptable, because a local velocity anomaly is expected due to the presence of older and more compacted folded sediments compared to the undeformed sediment drape. The hypothesis that the velocity anomaly is solely due to the presence of gas hydrate is therefore invalidated.

The thickness of free gas zone is variable in the investigated seismic data set. As noted in the Figure 9, the free gas zone is thicker (200 m) from 2.5 to 3.5 km in the model (nearby the BSR offset) where the concentration is about 3% $\pm$ 0.3%. Conversely, in the Eastern part, the concentration is highest (6% $\pm$ 0.3%) where the thickness is relatively lower (100–150 m).

The compressional velocity field is in agreement with previous studies in the area (see dotted thick lines in Figure 1; Tinivella et al. 1998; Tinivella and Accaino, 2000). Where the BSR is offset (at about 3.5 km in the model of Figure 3), it disappears for about 1 km in the proximity of a reverse fault that may be acting as a conduit for migration of gas and other fluids towards the surface.

The main conclusions that can be drawn from our analyses in the South Shetland Margin can be summarized as following:

(1) the velocity field above the BSR - in the first 500–600 m below the sea bottom - in the accretionary prism is quite uniform with some local positive anomalies related to the presence of particular geological structures (faults and folds) or gas hydrate;

(2) a free gas zone is present below the BSR with variable thickness;

(3) the velocity in the free gas zone is variable in the margin;

(4) considering the physical parameters described in Table 3, and supposing patchy distribution of free gas in the pore space, the average concentration of hydrate and free gas in the area is 6.0% $\pm$ 1.2% and 4.3% $\pm$ 0.3% of volume respectively;

(5) there are no evidence of BSR in the trench or in the continental shelf. The velocity analysis excludes also the occurrence of gas hydrates in these areas.

With the appropriate geological information on the control of geology versus hydrate cementation on the velocity field, a 2D-velocity seismic section can be interpreted as a gas hydrate and free gas concentration section. Ideally, borehole information on gas distribution is required to calibrate the model for estimation of concentrations to the punctual observation. In the case presented in this study, borehole information is not available and the model remains uncalibrated. The increasing availability quantitative borehole information of gas hydrates and free gas distribution with depth,

on multichannel seismic data of adequate quality will enable application of this methodology to other cases.

Acknowledgements

We are grateful to Aldo Vesnaver for valuable discussion. We thank Jacque Centonze and Nigel Wardell for the standard processing of seismic lines. We thank two anonymous reviewers for their constructive criticisms and valuable suggestions with respect to the presentation of this paper. We used the Seismic Unix package, provided by the Colorado School of Mines, to perform pre-stack depth migration. This work was supported by P.N.R.A. (Programma Nazionale di Ricerche in Antartide).

References

Andreassen, K., Mienert, J., Bryn, P. and Singh, S. C. 2000, A double gas-hydrate related bottom simulating reflector at the Norwegian Continental Margin. In Gerald D. Holder and P. R. Bishnoi (eds.), Gas Hydrates: Challenges for the Future, Proceedings of the Third International Conference in Gas Hydrates (July 18-22, 1999 - Salt Lake City, Utah), *Ann. NY Acad. Sci.* **912**, 126–136.

Barker, P. F., Camerlenghi, A., Acton, G. D. et al., 1999, *Proc. ODP, Init. Repts*, 178 [CD-ROM]. Available from: Ocean Drilling Program, Texas A&M University, College Station, TX 77845-9547, U.S.A.

Cochrane, G. R. and Cooper, A. K., 1991, Sonobuoy seismic studies at ODP drill sites in Pridz Bay, Antarctica. in J. Barron, B. Larsen et al. (eds.), Proc. ODP, Sci. Results, **119**, 27–45. College Station, TX (Ocean Drilling Program).

Domenico, S. N., 1977, Elastic properties of unconsolidated porous sand reservoirs. *Geophysics* **42**, 1339–1368.

Dvorkin, J., Moss, D., Packwood, J. L. and Nur, A., 1999, Identifying patchy saturation from well logs. *Geophysics* **64**, 1756–1759.

Fofonoff, N. P. and Millard, R. C. Jr., 1985, UNESCO Techical Papers in Marine Science, **44**.

Hamilton, E. L., 1978, Sound velocity gradients in marine sediments, *J. Acoust. Soc. Am.* **65**, 909–922.

Helgerud, M. B., Dvorkin, J., Nur, A., Sakai, A. and Collett, T., 1999, Elastic-wave velocity in marine sediments with gas hydrates: Effective medium modelling, *Geophys. Res. Lett.* **26(13)**, 2021–2024.

Hyndman, R. D., Yuan, T. and Moran, K., 1999, The concentration of deep sea gas hydrates from downhole electrical resistivity logs and laboratory data, *Earth Planet. Sci. Lett.* **172**, 167–177.

Hill, R., 1963, Elastic properties of reinforced solids: Some theoretical principles, *J. Mech. Phys. Solids* **11**, 357–372.

Klepeis, K. and Lowver, L. A., 1996, Tectonics of the Antarctic-Scotia plate boundary near Elephant and Clarence Islands, West Antarctica, *J. Geophys. Res.* **101**, 20,211–20,231.

Kim, Y. C., Samuelsen, C. M. and Hauge, T. A., 1996, Efficient velocity model building for prestack depth migration, *The Leading Edge* **15**, 751–753.

Kim, Y., Kim, H.-S., Larter, R. D., Camerlenghi, A., Gamba, L. A. P. and Rudowski, S., 1995, Tectonic deformation in the upper crust and sediments at the South Shetland trench. in Cooper, A. K. Barker, P. F. and Brancolini G. (eds.), *AGU Washington, D.C. Geology and Seismic Stratigraphy of the Antarctic Margin, Antarctic Research Series* **68**, 157–166.

Kuster, G. T. and Toksöz, M. N., 1974, Velocity and attenuation of seismic waves in two-phase media: Part I. Theoretical formulations, *Geophysics* **52**, 1391–1401.

Larter, R. D. and Barker, P. F., 1991, Effects of ridge crest-trench interaction on Antarctic-Phoenix spreading: Forces on a joung subducting plate, *J. Geophys. Res.* **96**, 19,583–19,607.

Lodolo, E., Camerlenghi, A. and Brancolini, G., 1993, A bottom Simulating reflector on the South Shetland margin, Antarctic Peninsula, *Antarctic Sci.* **5(2)**, 201–210.

Lodolo, E., Camerlenghi, A., Madrussani, G., Tinivella, U. and Rossi, G., 2002, Assessment of gas hydrate and free gas distribution on the South Shetland margin (Antarctica) based on multichannel seismic reflection data, *Geophys. J. Internl.* **148**, 103–119.

Maldonado, A., Larter, R. D. and Aldaya, F., 1994, Forearc tectonic evolution of the South Shetland Margin, Antarctic Peninsula, *Tectonics* **13**, 1345–1370.

Miles, P. R., 2000, Geophysical sensing and hydrates. in M. D. Max (ed.), *Natural Gas Hydrates in Oceanic and Permafrost Environments*, Kluwer Academic Publishers, Dordrecht, 261–274.

Paull, C. K., Matsumoto, R., Wallace, P. J. and Dillon, W. P., (eds.), 2000, Proc. ODP, Sci. Results, 164 [Online]. Available from World Wide Web: <http://www-odp.tamu.edu/publications/164_SR/164TOC.HTM>.

Riley, J. P. and Chester, R., 1987, *Introduction to Marine Chemistry*. Accademic Press, London.

Shipboard Scientific Party, 1999, Shelf Transect (Sites 1100, 1102, and 1103), in Barker, P. F., Camerlenghi, A., Acton, G. D. et al., Proc. ODP, Init. Repts., 178, 1-83 [CD-ROM]. Available from: Ocean Drilling Program, Texas A&M University, College Station, TX 77845-9547, U.S.A.

Tinivella, U., 1999, A method for estimating gas hydrate and free gas concentrations in marine sediments, *Bollettino di Geofisica Teorica ed Applicata* **40(1)**, 19–30.

Tinivella, U. and Accaino, F., 2000, Compressional velocity structure and Poisson's ratio in marine sediments with gas hydrate and free gas by inversion of reflected and refracted seismic data (South Shetland Islands, Antarctica), *Marine Geol.* **164**, 13–27.

Tinivella, U., Camerlenghi, A. and Rebesco, M., 2001, Data report: Seismic velocity analysis on the continental shelf transect, ODP Leg 178, Antarctic Peninsula. in P. F., Barker, A., Camerlenghi, G. D., Acton and A. T. S., Ramsay (eds.), Proc. ODP, Sci. Results, 178 [Online]. Available from World Wide Web: <http://www-odp.tamu.edu/publications/178_SR/chap_16/chap_16.htm>.

Tinivella, U. and Carcione, J. M., 2000, Estimation of gas-hydrate concentration and free-gas saturation from log and seismic data *SEG, Expanded Abstract [CD-ROM].*

Tinivella, U. and Lodolo, E., 2000, The Blake Ridge BSR transect: Tomographic velocity field and theoretical model to estimate methane hydrate quantities. in C. K. Paull, R. Matsumoto, P. J. Wallace and W. P. Dillon (eds.), *Proceedings of the Ocean Drilling Program, Scientific Results*, Vol. **164**. [Online]. Available from World Wide Web: Available from World Wide Web: http://www-odp.tamu.edu/publications/164_SR/chap_28/chap_28.htm

Tinivella, U., Lodolo, E., Camerlenghi, A. and Bohem, G., 1998, Seismic tomographic study of a bottom simulating reflector off

the South Shetland Islands (Antarctica). in J.-P. Henriet and J. Miniert (eds.), *Gas hydrates: relevance to World Margin Stability and Climate Change*, Vol. **137**, pp. 141–151. Geological Society, London, Special Publication.

Wood, W. T. and Ruppel, C., 2000, Seismic and thermal investigations of the Blake Ridge gas hydratearea: a synthesis. in C. K., Paull, R., Matsumoto, P. J., Wallace and W. P., Dillon (eds.), Proc. ODP, Sci. Results, **164**, [Online]. Available from World Wide Web: <http://www-odp.tamu.edu/publications/164_SR/VOLUME/CHAPTERS/SR164_26.PDF>

Yilmaz, Ö., 2001, Seismic data analysis. Processing, inversion, and interpretation of seismic data. *Society of Exploration Geophysicists*, *Ser Investig. Geophys.* **10**, Tulsa, OK.

Yuan, T., Spence, G. D., Hyndman, R. D., Minshull, T. A. and Singh, S. C., 1999, Seismic velocity studies of a gas hydrate bottom-simulating reflector on the northern Cascadia continental margin: Amplitude modelling and full waveform inversion, *J. Geophys. Res.* **104(B1)**, 1179–1191.

Zelt, C. A. and Smith, R. B., 1992, Seismic traveltime inversion for 2-D crustal velocity structure, *Geophys. J. Int.* **108**, 16–34.